Calculations of the geometry and optical properties of F_{Mg} centers and dimer (F_2-type) centers in corundum crystals

E. A. Kotomin,* A. Stashans,† L. N. Kantorovich, A. I. Lifshitz, A. I. Popov, and I. A. Tale

University of Latvia, 19 Rainis Blvd., Riga, LV-1050, Latvia

J.-L. Calais

Department of Quantum Chemistry, Uppsala University, Box 518, S-571 20, Uppsala, Sweden

Results of the defect calculations in α-Al$_2$O$_3$ (corundum) crystals using the semiempirical method of intermediate neglect of differential overlap and large, 65-atom-stoichiometric quantum clusters are reported. The geometry and the electronic density distribution are simultaneously and self-consistently optimized for both the ground and excited states of the electronic F_{Mg}, F_{Mg}^- single centers and two kinds of dimer (F_2, F_2^+, F_2^{2+}) centers where two oxygen vacancies belong to the same basic oxygen triangle and are next nearest neighbors on adjacent basal planes, respectively. Their optical absorption and luminescence energies are compared with available experimental data; absorption bands are predicted. Positions of dimer-center local levels within the gap of the perfect crystal are calculated.

I. INTRODUCTION

Corundum (α-Al$_2$O$_3$) is an important technological material which is utilized as a host material for solid-state lasers, fusion reactors, ceramics, γ dosimetry,[1-4] etc. This is why the nature of point defects and how they affect the optical properties of corundum have stimulated large number of experimental studies.[5,6] The basic electronic point defects in corundum are single-vacancy F^+ and F centers (one and two electrons in an oxygen vacancy) and dimer F_2^{2+}, F_2^+, and F_2 centers [two nearest-neighbor (NN) or next-NN (NNN) oxygen vacancies trapping from 2 to 4 electrons; the superscript shows the defect effective charge with respect to the perfect lattice].[5-10] Only a few theoretical attempts have been made up to now to understand the properties of F-type centers;[10-13] and there are no theoretical studies of dimer centers so far to our knowledge. In our previous short paper[14] a semiempirical quantum-chemical method was used for cluster calculations of F^+ and F centers. We focused there on self-consistent calculations of single-vacancy-defect geometry and optical properties. Good agreement with the experimental data on both absorption and luminescence energies encouraged us to extend these calculations now to a detailed study of impurity-related centers, the so-called F_{Mg} centers, and a family of intrinsic dimer centers. We are fully aware of the limitations of our computational methods but would like to stress that (i) they have yielded good results in defect studies in both semiconductors[15] and a series of wide-gap oxides[16] (MgO, Li$_2$O, SiO$_2$); (ii) due to time-saving semiempirical methods we are able to sift through the vast number of possible models until one or two prospective models are caught for more detailed study by first-principles methods; (iii) we focus more on qualitative understanding of the physical effects and underlying physical processes. In particular, in Ref. 14 we have demonstrated in a very

simple way that the considerable splitting of the absorption bands observed in the F^+ center and the lack of splitting in the F center come out directly from the localized and delocalized nature of their excited states, respectively. Section II of this paper contains a description of the computational procedure, in Sec. III we give our main results, whereas Sec. IV presents discussion and conclusions.

II. COMPUTATIONAL METHOD

The semiempirical quantum-chemical method of the intermediate neglect of differential overlap (INDO) was used here;[17] its modification for defect studies in ionic and semi-ionic solids is described in detail in Refs. 16. A large stoichiometric cluster of 65 atoms was used as shown in Fig. 1. This cluster was embedded into the electrostatic field of a nonpoint-ion rigid lattice. The valence basis set included 3s and 3p atomic orbitals (AO's) on Al and 2s and 2p on O atoms. The INDO parameters were first calibrated to reproduce correctly the basic properties of 12 small Al- and O-containing molecules (AlO, AlCl, AlO$_2$, Al$_2$O, Al$_2$, Al$_2$O$_3$, O$_2^-$, etc.), as well as the band structure and lattice parameters of a pure corundum crystal. These parameters were used already successfully in the INDO studies of small-radius hole polarons in corundum crystals.[18] For perfect corundum the effective charges on the ions are: $+2.34e$ (Al) and $-1.56e$ (O), which confirm previous experimental[19] and theoretical[20] conclusions about the semi-ionic nature of its chemical bonding. The upper valence band is mixed and formed mainly by the O ($2p$) and Al ($3p$) AO's. We recall that the structure of perfect corundum is hexagonal close packing of O ions with Al ions occupying $\frac{2}{3}$ of the octahedral interstices. Each Al ion has three nearest-neighboring O ions at a distance 1.86 Å and three next-NN O ions at a distance 1.97 Å. Each O ion is surround-

ed by four Al ions, two at each of these distances. Löwdin's population analysis shows that the O-O bonds in our pure-corundum calculations are not populated but the two kinds of Al-O short and long bonds just mentioned are populated by $0.28e$ and $0.17e$, respectively. Good illustrations of the corundum structure are given in Refs. 6 and 20; its top view is shown in Fig. 1.

In F-center-type calculations we extended the basis set by centering at the O vacancy additional AO's ($1s$ and $2p$ for the ground and excited states, respectively). Their parameters are given in Ref. 14; note here that the only fitting used was done for the orbital exponents of the F^+ wave function in order to reproduce the experimental energy of the central absorption band at 5.5 eV ($1A \rightarrow 2A$ transition). The same basis set has been used successfully in the same paper for F-center calculations and is used in this paper for impurity-induced F_{Mg} and dimer centers. The absorption and luminescence energies are obtained as
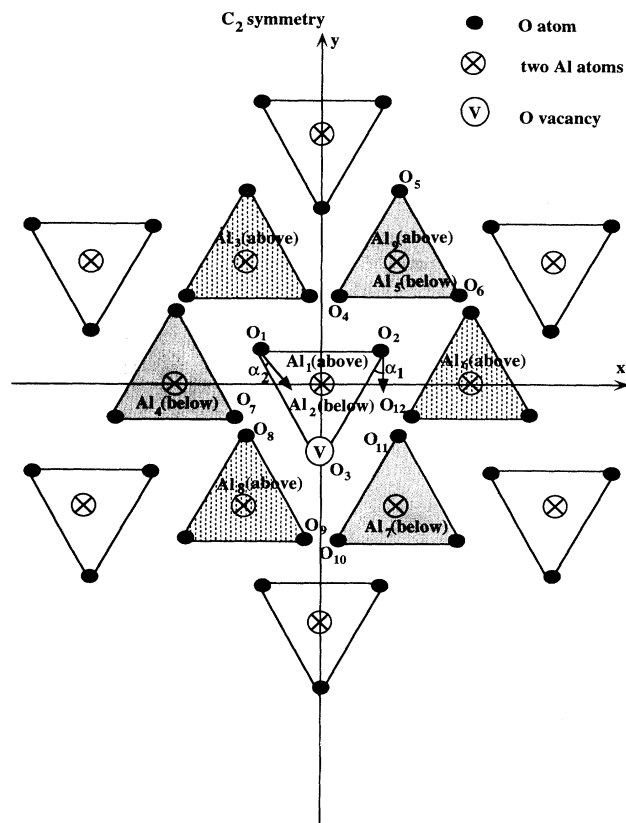
the difference of total energies for the self-consistent-field ground and excited states for optimized defect geometry (ΔSCF method). That is, the potential-energy curves are calculated for the ground and excited states of defects; then according to the Frank-Condon principle the absorption energy is that for the vertical transition from the minimum of the relaxed ground state to the SCF excited state (i.e., for a fixed atomic configuration). The luminescence energy is calculated as the vertical transition from the minimum of the relaxed excited state to the ground-state curve. Note that these ΔSCF energies do not coincide with the difference of the relevant one-electron (orbital) energies, which usually give only rough estimates for the absorption and luminescence energies. For simplicity we use notations for one-electron energies in tables presenting results of SCF calculations.

For low-symmetric and complicated structures like corundum crystals (F centers have only C_2 symmetry) it is important (i) to use as much as possible an automated search for the optimal defect geometry, which is usually far from self-evident, as in alkali halides, where F centers have O_h symmetry; (ii) to use maximally the point symmetry of defects (as well as of the periodic crystal) in order to calculate quantum clusters as large as possible, where defects in the center would not be affected by the cluster boundary effects. Both these conditions are met in the SYM-SYM INDO computer code used in this paper.[21,22]

In calculations of the excited states of low-symmetry defects there is a potential danger that SCF calculations converge to the ground state due to the nonorthogonality of the wave functions of the ground and excited states (the effect called "the variational collapse" and observed by us more than once). However, this was not observed in the present calculations since (i) even in the worst case of dimer (F_2) NNN centers discussed below and having no point symmetry at all, their ground-state and excited-state wave functions are still well orthogonal, being of s and p nature, respectively; (ii) the energy gap between the relevant energy levels during the SCF procedure remains considerable (> 4 eV) whereas the collapse usually occurs when, after a certain number of SCF iterations, the one-electron energy of the excited state critically approaches that of the (virtual) ground state. Therefore the reliability of the excited-state energy calculations in our particular case is not affected by their low symmetry.

Although physically equivalent to our previous semiempirical INDO code CLUSTER described elsewhere,[16] the SYM-SYM code has the advantage of being much more efficient in both the electronic structure and geometry optimization calculations, because of the complete account of the point symmetry built into the code.[21] The modified version of the INDO method used by us differs from the "standard" one by Pople and Beveridge[17] mainly in the facts that (i) atomic orbitals of different atomic shells (s, p, and d types) may have different principal quantum numbers which allows us to treat, for example, d elements, such as Ag, Ti, and Zr and (ii) the interaction of electrons with atomic cores is described by a special kind of pseudopotential containing additional adjustable parameters. The residual part of the crystal located out

FIG. 1. Top view of the stoichiometric quantum cluster used in the calculations. It contains 13 structural elements (SE's); each SE includes a five-ion oxygen triangle and two Al atoms situated symmetrically above and below the triangle, on the z axis perpendicular to the triangle plane. The cluster consists of three basal planes shown in white, dots (2.17 Å below the xy plane), and gray (2.17 Å above the xy plane), respectively. In F-type defect calculations the ion O_3 was replaced by a vacancy. Dimer centers contain two NN and NNN vacancies on adjacent planes (see Figs. 2 and 3 below for more details).

of the molecular cluster (MC) is considered in the nonpoint-charge approximation: the Coulomb interaction of the MC electrons with adjacent boundary atoms is considered in the same manner as that for the atoms lying inside the MC (i.e., using the density matrix of the perfect crystal obtained in a separate calculation and taking into account explicitly the AO's of the outside atoms), whereas atoms which are far away from the MC are considered as point-charge-like. The contribution of the infinite number of the latter atoms is calculated exactly making use of the Ewald method.[23] The matrix elements of the total Coulomb field produced by the nonpoint-charge outer region, as described above, are added to the diagonal elements of the Fock matrix of the MC.

The self-consistent procedure (SCP) is performed in the following way. Based on the point group G of the MC specified in the input, the code constructs the symmetry-adapted orbitals (SAO's) as corresponding linear combinations of AO's of symmetry-related atoms; the latter will be called *orbits* hereafter. Note that all MC atoms can be unambiguously split into orbits with respect to the symmetry adopted. Using the transformation matrix AO→SAO, the corresponding similar transformation is performed for the Fock matrix which in the SAO representation is obtained for every irreducible representation (IR) Γ of the group G. These Fock matrices are usually not of very large dimensions and are diagonalized rapidly. Making use of the eigenvectors thus obtained for every IR, the density matrix (=bond-order matrix) of the MC in the SAO representation is calculated, which (on the next step) is transformed to the AO representation by the same similarity transformation as described above. Then the new portion of the Fock matrix is calculated and the cycle is repeated unless convergency is achieved.

Several comments have to be made here. First of all, we note that it was found to be less convenient and much more expensive to use the expression for the Fock matrix directly in the SAO representation. Instead, it turned out to be more efficient to perform AO→SAO and SAO→AO transformations, as described above. This is because of the fact that in the SAO representation the Fock matrix has in general a complicated expression in spite of the INDO method applied here. Another point is that all matrices needed for the calculations and used in the AO representation (the Fock, overlap, density matrices, and two-center Coulomb integrals) are stored in portions which are related to the first atoms of orbits. This allows us to save substantially in the required computer memory.

A special procedure was developed in the code in order to make the geometry optimization process as fast and efficient as possible. First of all, the symmetry allows us to reduce the optimizing space to that spanned by the coordinates of the first atoms of all orbits. Moreover, depending on the positions of these atoms with respect to the symmetry elements, we have a limited number of degrees of freedom for every orbit: (i) 0 if the atom is located in the center of symmetry, i.e., when inversion takes place; (ii) 1 if the atom is on an axis; (iii) 2 if it is on a plane; (iv) 3, a general position. In order to develop an automated algorithm combining all the cases mentioned

above, we have to construct the normal coordinates $\Lambda_{\xi f}^{\mu}$ for every IR Γ of the group G for every orbit ξ (f distinguishes equivalent IR's):

$$\Lambda_{\xi f}^{(\Gamma)} = \sum_{A \in \xi} \sum_{\alpha} W_{\xi f, A\alpha}^{(\Gamma)} \Psi_{\xi A\alpha} , \tag{1}$$

where the elements $\{W_{\xi f, A\alpha}^{(\Gamma)}\}$ represent the corresponding transformation matrix, and the summation in Eq. (1) is carried out over all atoms A from the orbit ξ and also over all Cartesian components $\alpha = x, y, z$ of the atomic displacement vectors $\mathbf{u}_{\xi A} = \mathbf{R}_{\xi A} - \mathbf{R}_{\xi A}^0$. The coefficients $W_{\xi f, A\alpha}^{(\Gamma)}$ can easily be found by means of group theory for every IR Γ.[21] They can always be chosen in such a way that the matrix W is orthogonal, i.e.,

$$\sum_{\Gamma} \sum_{\xi f} W_{\xi f, A\alpha}^{(\Gamma)} W_{\xi f, A'\alpha'}^{(\Gamma)} = \delta_{AA'} \delta_{\alpha\alpha'} . \tag{2}$$

In order to maintain the system symmetry unchanged during the geometry optimization process, we must set all normal coordinates $\Lambda_{\xi f}^{(\Gamma)}$ to vanish except ones belonging to the unique symmetrical IR A_1:

$$\Lambda_{\xi f}^{(\Gamma)} = \begin{cases} \Lambda_{\xi f}, & \Gamma = A_1 , \\ 0, & \Gamma \neq A_1 . \end{cases} \tag{3}$$

The above-written formulas allow us to solve Eq. (1) with respect to the displacement vector $\mathbf{u}_{\xi 1}$ of the first atom of an arbitrary orbit ξ:

$$R_{\xi 1\alpha} = R_{\xi 1\alpha}^0 + \sum_{f} W_{\xi f, 1\alpha}^{(A_1)} \Lambda_{\xi f} . \tag{4}$$

The total number of $\Lambda_{\xi f}$'s gives the minimal possible number of independent coordinates of the system. Equation (4) can be used as the desired link between the actual optimization variables $\Lambda_{\xi f}$ and the real coordinates of the atoms in the system, $R_{\xi 1\alpha}$, used in the input of the computer (all other atoms of every orbit are produced by the group operations).

Then we have found that the usual optimization strategy to minimize the system energy with respect to all variables $\{\Lambda_{\xi f}\}$ simultaneously turned out to be inefficient for most of the cases considered here. Another, more efficient algorithm has been developed. The code performs a loop over orbits ξ and carries out independent optimization for every orbit, which is never larger than a three-dimensional optimization. At every step (every calculation of the system energy) the bond-order matrix found on the previous step is used as the initial guess; in addition, only such integrals are actually recalculated which are connected with the current orbit ξ under question. These two circumstances substantially accelerate energy calculations. The loop is repeated until convergency with respect to the system coordinates is achieved. In addition, we have found that it is quite useful to specify different levels of optimization for every orbit in question. Indeed, let us consider an orbit ξ lying far away from the defect (on the periphery of the MC). Ions of this orbit are shifted only slightly and their influence on the defect electronic density is not very great. This means that we can ignore the SCP while ob-

taining the cluster energy during the optimization procedure of the orbit ξ. Thus for these orbits we can limit ourselves to the calculation of the system's energy based on the bond-order matrix found on the previous self-consistent step. In addition, all two-center integrals connected with this orbit must be recalculated (their number is not very large). Therefore this energy calculation procedure can be performed very economically as an independent part of the code.

Then, if an orbit ξ is considered which is closer to the defect region but still is out of it, the SCP can still be ignored during the individual orbit optimization as in the previous case. However, after the end of the optimization the complete SCP is performed in order to renew the density matrix.

Lastly, if an orbit lies directly in the defect region, the complete SCP has to be done for every energy calculation during the optimization since any (sometimes even small) shift of ions may result in substantial electronic density redistribution.

The optimization strategy described above leads to a larger number of optimization steps and to a larger number of individual calculations of the cluster energy. However, every such calculation demands, on average, less computer time than the complete SCP. That is why we have considerable gain in computational time.

III. RESULTS

A. Mg-related F centers

Several experimental studies[6,24,25] were devoted to the F-type centers in Mg-doped corundum. Since there are two kinds of Al-O bonds, two kinds of F(Mg) centers with a Mg^{2+} ion substituting for an Al^{3+} ion near an oxygen vacancy could also exist. However, since the difference in their bond lengths is small, we calculated properties of F(Mg) centers for the shortest Al-O bonds which corre-

TABLE I. Relaxation of ions surrounding F_{Mg} and F_{Mg}^- centers (in % of the interatomic distances) (Mg atom substitutes for Al_7; see Fig. 1). F_{Mg} and F_{Mg}^- centers are F^+ and F centers having in their nearest vicinity the Mg^{2+} ion substituting for a regular Al^{3+} ion. The $+$ sign denotes displacements of atoms towards and $-$ away from a vacancy; the angles α_1 and α_2 are shown in Fig. 1. GS and ES denote the ground and excited states, respectively.

		F_{Mg} center	F_{Mg}^- center
O_1	GS	$+4.3$, $\alpha_2 = 14°$	$+0.7$, $\alpha_2 = 25°$
	ES	$+4.7$, $\alpha_2 = 16°$	$+0.7$, $\alpha_2 = 25°$
O_2	GS	$+2.5$, $\alpha_1 = 23°$	-0.5, $\alpha_1 = 12°$
	ES	$+3.8$, $\alpha_1 = 22°$	-0.5, $\alpha_1 = 12°$
Al_1, Al_2	GS	-8.9	-3.7
	ES	-10.8	-5.4
Al_7, Al_8	GS	-2.4	$+0.8$
	ES	-3.2	$+0.3$
Mg	GS	$+4.1$	$+10.3$
	ES	$+6.7$	$+12.5$

TABLE II. Absorption and luminescence energies (in eV) for Mg-related centers and dimer centers in the case when the oxygen vacancies lie in different oxygen planes (in both cases the point group symmetry is C_1). These energies are calculated using the ΔSCF procedure.

	F_{Mg}	F_{Mg}^-	F_2	F_2^+	F_2^{2+}
	Absorption				
$1A \rightarrow 2A$	5.1	6.35	5.0	4.5	4.1
$1A \rightarrow 3A$	5.3	6.4	5.1	4.6	4.2
$1A \rightarrow 4A$	5.9	6.5	5.4	4.7	4.3
Expt. (Ref. 9)			4.1	3.5	2.7
Expt. (Refs. 26,27)	4.95, 5.7				
	Luminescence				
	4.2	3.5	4.4	3.9	3.5
Expt. (Ref. 9)			3.85	3.27	2.25
Expt. (Ref. 26)	4.1				

spond to the pair O_3-Al_7 in Fig. 1. Another problem is what is the net charge of this defect, i.e., is it Mg^{2+} near the F^+ center (neutral pair) or near the F center (denoted hereafter F_{Mg} and F_{Mg}^-, respectively)?

Table I gives the optimized geometry for both centers, F_{Mg} and F_{Mg}^-, whereas Table II summarizes calculated absorption and luminescence energies. The atomic relaxations for these two defects are quite different, very likely due to the negative net charge of the F_{Mg}^- center. In the neutral F_{Mg} center the O_1 and O_2 ions are displaced slightly more than in the F center (2.2%) but less than in F^+ (4.6%),[14] and by quite different angles. Al_1 and Al_2 displacements are slightly larger due to the Coulomb repulsion from the O vacancy. The Mg^{2+} ion itself is displaced towards the F^+ center, since it is oppositely charged with respect to the perfect crystal lattice.

Inspection of the calculated absorption energies shows that definitely only the F_{Mg} center fits the experimental values. Thus we predict a third absorption band to exist. In the F_{Mg} absorption the transitions $1A \rightarrow 2A$, $3A$, and $4A$ occur between the electronic states predominantly consisting of s AO's centered on a vacancy and p_z, p_y, and p_x states [coefficients in the molecular orbitals (MO's) are 0.97 for the ground state and 0.72, 0.46, and 0.54 for the three excited states, respectively]. The

TABLE III. Absorption and luminescence (ΔSCF) energies (in eV) for F^+ and F centers (Ref. 14).

		INDO	Expt. (Refs. 5,6)
		Absorption	
F^+	$1A \rightarrow 1B$	5.2	4.8
	$1A \rightarrow 2A$	5.5	5.4
	$1A \rightarrow 2B$	5.8	6.0
F	$1A \rightarrow 2A$	5.9	6.1
		Luminescence	
F^+	$1B \rightarrow 1A$	4.0	3.8
F	$2A \rightarrow 1A$	2.8	3.0

TABLE IV. Effective charges of ions (in units of e) surrounding Mg-related F centers and dimer centers (both oxygen vacancies lie in the same triangle) (see Fig. 2).

	Perfect crystal	F_{Mg}	F_{Mg}^-	F^-	F_2	F_2^+	F_2^{2+}
O_1,O_2,O_3	-1.57	-1.54	-1.53	-1.54	-1.50	-1.51	-1.50
Al_1,Al_2	2.35	2.27	2.31	2.32	2.34	2.27	2.21
Al_3,Al_4,Al_5,Al_6	2.36	2.29	2.32	2.32	2.35	2.34	2.30
Al_7,Al_8	2.36				2.16		
Number of trapped electrons, in a vacancy		-0.94	-1.82	-1.68	-1.75	-1.37	-0.94
Mg^a		1.93	1.94				

[a]Mg substitutes for Al_7; see Fig. 1.

relevant absorption and luminescence energies for F^+ and F centers are given in Table III. Here the states $1A$, $1B$, $2A$, and $2B$ consist mainly of s AO's centered on the vacancy and of p_z, p_y, and p_x excited AO's, respectively.

The charge distribution analysis shown in Table IV indicates that in both centers the Mg ion has the effective charge ≈ 1.9 eV, the oxygen vacancy trapped $0.9e$ and $1.8e$, respectively, and the charges of the surrounding ions are close to those in perfect corundum, i.e., we have a purely Coulomb effect of Mg^{2+}-F^+ interaction, shifting the F_{Mg} ground-state level to 3.7 eV above the top of the valence band (as compared to 3.1 eV for the isolated F^+ center). Since the ground state of the F_{Mg}^- center lies considerably higher than that for the F_{Mg} center, 4.8 eV above the top of the valence band [similarly to the case of the F center, 5.3 eV (Ref. 14)], the excited states of F_{Mg}^- fall into the conduction band and due to their delocalized nature no longer reveal splitting into three bands as F^+ or F_{Mg} centers do; see Sec. IV and Ref. 14 for more details.

B. Dimer centers with oxygen vacancies lying in the same oxygen triangle (NN case)

The relaxations of ions surrounding dimer centers when two oxygen vacancies are NN's and lie in the same basic oxygen triangle (whose plane is perpendicular to the z axis) are drawn schematically in Fig. 2 and given numerically in Table V whereas their absorption energies

are plotted in Table VI. One can see that an increase of the dimer-center net charge from zero to $+2$ (in the series $F_2 \rightarrow F_2^+ \rightarrow F_2^{2+}$) leads to a considerable increase of the ionic displacements, due to the Coulomb interaction between surrounding ions. These centers have not been studied experimentally so far to our knowledge, but based on calculations we predict the same trend in the absorp-
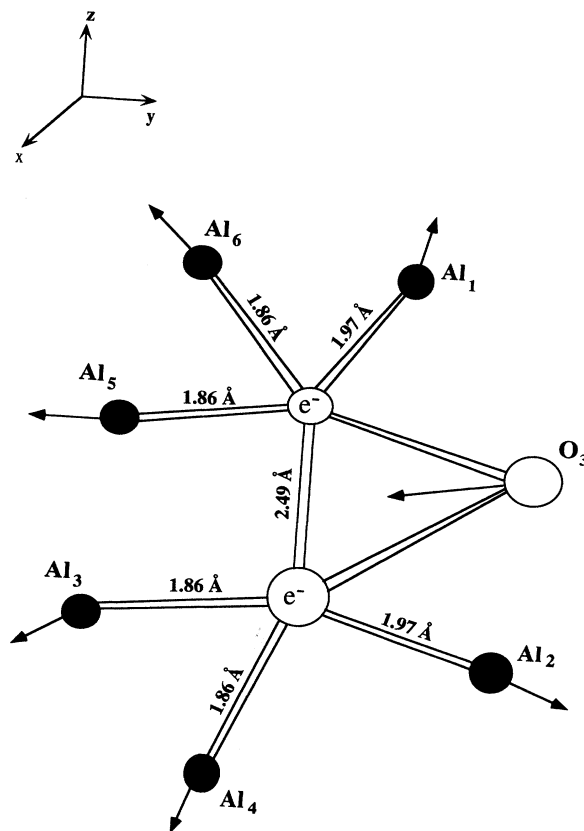
FIG. 2. Calculated relaxations of ions surrounding a dimer center where two vacancies are NN's within the basic oxygen triangle.

TABLE V. Relaxation of surrounding ions (in % of the interatomic distances) for dimer centers, if two oxygen vacancies are NN's, i.e., belong to the same oxygen triangle (see Fig. 2). The $+$ sign denotes displacements of atoms towards and the $-$ sign away from a vacancy; GS and ES are the ground and excited states, respectively.

		F_2	F_2^+	F_2^{2+}
O_3	GS	$+9.0$	$+14.4$	$+19.6$
	ES	$+11.2$	$+17.8$	$+22.3$
Al_1,Al_2	GS	-6.2	-9.2	-12.8
	ES	-8.8	-12.4	-15.5
Al_3,Al_4,Al_5,Al_6	GS	-2.8	-5.3	-7.7
	ES	-3.5	-7.9	-10.2

TABLE VI. Calculated absorption and luminescence energies (ΔSCF, in eV) for dimer centers in the case when both oxygen vacancies belong to the same oxygen triangle (symmetry C_2). Optical transitions are allowed (in the dipole approximation) only for light polarized along the directions given in the parentheses. The two vacancies lie on the y axis.

	F_2	F_2^+	F_2^{2+}
	Absorption		
$1A \rightarrow 1B$ (x,z)	4.6	3.8	2.9
$1A \rightarrow 2A$ (y)	5.4	3.9	a
$1A \rightarrow 2B$ (x,z)	5.5	4.3	3.0
	Luminescence		
$1B \rightarrow 1A$ (x,z)	4.2	3.5	2.7

[a]No convergence achieved.
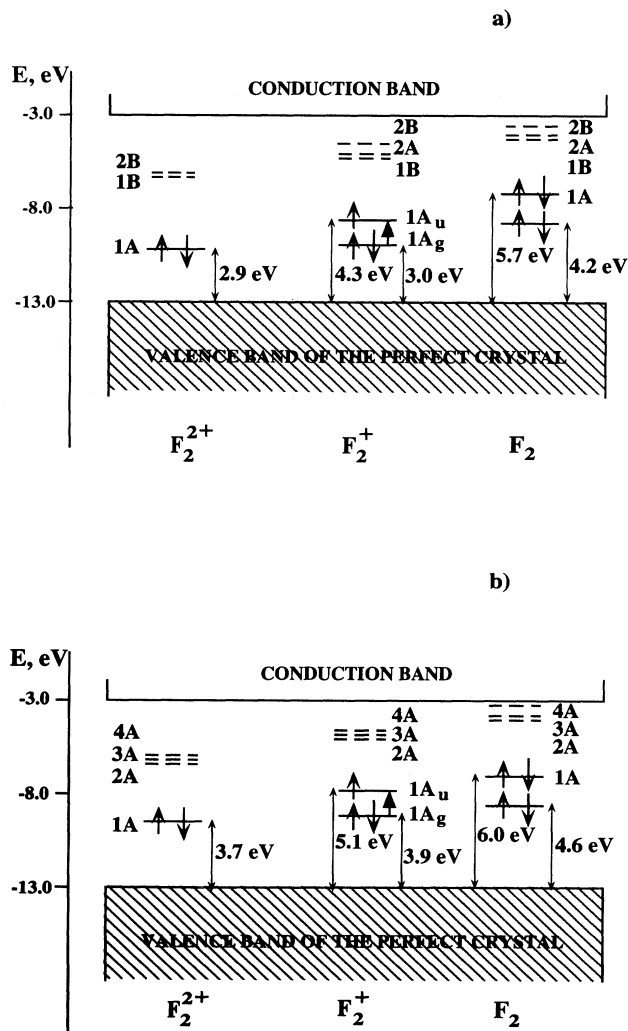
FIG. 3. Positions of the one-electron dimer levels within the corundum gap for the cases when the two vacancies are NN's (a) and NNN's (b). Dashed lines denote SCF energies for the excited states with the geometry corresponding to the relaxed ground state. The bold arrow shows the M-type transition observed earlier for F_2 centers in alkali halides (see text).

tion and luminescence energies as is observed for another type of dimer centers discussed in Sec. III C; namely, their decrease in the series $F_2 \rightarrow F_2^+ \rightarrow F_2^{2+}$ (Table VI). The strong conformation effects in corundum are seen from the larger displacements of the atoms surrounding vacancies when they belong to the same oxygen triangle, in comparison to shifts of the corresponding atoms in similar centers when the vacancies lie in two adjacent basal planes. In the first case the structural element Al$_2$O$_3$ of the perfect corundum structure is destroyed almost completely by removing two O atoms from the basic oxygen triangle, which leads to considerable displacements occurring due to the broken bonds. In contrast, in the NNN case only a few bonds within each of the oxygen triangles entering the SE were broken while the SE's themselves have not been destroyed; thus the relaxation of atoms within the two SE's is smaller.

A simple group-theoretical analysis of the selection rules for absorption and luminescence of these centers (C_2 symmetry without a center of symmetry) shows that in the dipole approximation only some optical transitions are allowed; the related light polarization is indicated in Table VI in parentheses. This could be used for discrim-
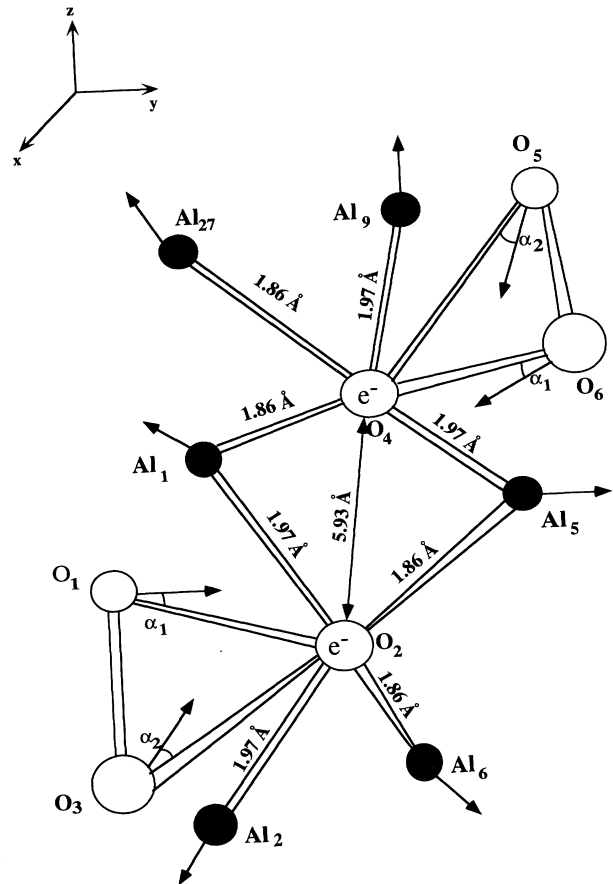
FIG. 4. Ionic relaxation for the dimer center where two vacancies are NNN's belonging to the nearest basal planes.

TABLE VII. Relaxation of surrounding ions (in % of interatomic distances) for dimer centers, if two oxygen vacancies are NNN's, i.e., belong to different triangles and lie in two different oxygen planes (see Fig. 3). Ions Al_1 and Al_5 are NN to both vacancies whereas Al_2 and Al_9 belong to the same structural element as a vacancy and ions Al_6, Al_{27} belong to another structural element.

		F_2	F_2^+	F_2^{2+}
O_3, O_5	GS	$+1.7$, $\alpha_2 = 11°$	$+5.5$, $\alpha_2 = 7°$	$+8.2$, $\alpha_2 = 10°$
	ES	$+2.2$, $\alpha_2 = 11°$	$+6.1$, $\alpha_2 = 7°$	$+9.4$, $\alpha_2 = 10°$
O_1, O_6	GS	$+1.3$, $\alpha_1 = 6°$	$+3.4$, $\alpha_1 = 5°$	$+4.7$, $\alpha_1 = 5°$
	ES	$+1.8$, $\alpha_1 = 6°$	$+4.0$, $\alpha_1 = 5°$	$+5.6$, $\alpha_1 = 5\%$
Al_1, Al_5	GS	-0.8	-3.2	-4.7
	ES	-1.1	-3.2	-5.5
Al_2, Al_9	GS	-1.4	-3.2	-6.6
	ES	-1.6	-4.0	7.4
Al_6, Al_{27}	GS	-0.6	-2.0	-3.9
	ES	-0.9	-2.6	-4.5

ination of the symmetry of these excited states, as well as identification of the NN dimer centers. Analysis of the relevant wave functions for all three kinds of dimer centers (F_2, F_2^+, F_2^{2+}) shows that $1A$ states consist predominantly of s AO's centered on vacancies, whereas $2A$, $1B$, and $2B$ states consist mainly of p_y, p_z, and p_x AO's (each of two vacancies contributes to the MO with coefficients close to 0.6–0.7 thus indicating strong localization of both ground and excited states for all three dimer defects).

Positions of the (orbital) one-electron energy levels for both the ground and unrelaxed excited states are plotted in Fig. 3(a). The latter SCF states shown by the dashed lines correspond to atomic configuration optimized for the relaxed ground state and thus the distance between the ground-state level and excited-state level characterizes the optical absorption. The procedure of placing defect levels with respect to the perfect crystal bands is described in Ref. 16. It is based on matching the midpoints of the deep $2s$ O bands obtained for the perfect crystal and in a defect-cluster calculation. The effective charges of ions given in Table IV show no appreciable charge redistribution effects as compared to the perfect corundum crystal; the two vacancies have trapped almost entirely $4e$, $3e$, and $2e$, respectively. The rest of the electron density $(0.5e)$ is spread out over the nearest ions.

C. Dimer centers with oxygen vacancies lying in the two adjacent basal planes (NNN case)

This kind of dimer center has been studied experimentally;[7,9] Table VII presents the calculated ionic displacements (visualized in Fig. 4). The calculated optical transitions are compared with the experimental data in Table II.

The conclusion could be drawn from Table VIII that in these dimer centers, as compared to their counterparts in Sec. III B, charge density is more delocalized from the two vacancies over the nearest cluster atoms. The positions of dimer-center local energy levels in the gap of perfect corundum [Fig. 3(b)] are higher in energy than for NN dimers for both the ground and excited states.

IV. DISCUSSION AND CONCLUSIONS

In a series of calculations on various basic electronic centers in corundum crystals presented in this and a previous paper,[14] we have investigated systematically the intrinsic F^+, F, and Mg-impurity-related electronic centers. The semiempirical method used here combined

TABLE VIII. Effective charges of atoms (in units of e) surrounding dimer centers if the two oxygen vacancies are in different basal planes (see Fig. 3).

	Perfect crystal	F_2	F_2^+	F_2^{2+}
O_1, O_3, O_5, O_6	-1.57	-1.51	-1.52	-1.53
Al_2, Al_9	2.35	2.34	2.30	2.29
Al_1, Al_5	2.35	2.33	2.28	2.16
Al_6	2.36	2.35	2.30	2.51
Number of trapped electrons per vacancy		-1.75	-1.13	-0.75

with an automated search for the optimal geometry of defects turned out to be a very useful tool for defect simulations in corundum aimed to check theoretically their models and optical properties. The absorption and emission energies for single-electron centers F^+ and F were found in Ref. 14 to be in very good agreement with the experimental data, and the same is true for the activation energy for thermal quenching of F^+ luminescence.

We demonstrated there that the observation of the triple splitting of the excited state of the F^+ center and its absence for the F and hypothetical F_{Mg}^- centers are directly related to the degree of spatial localization of the excited state. It might be easily demonstrated that the low-symmetry crystalline field $V(r)$ has a much smaller effect on the excited electronic states Ψ, when its matrix elements $\langle \Psi | V | \Psi \rangle$ are smaller. This is the case when F-type excited wave functions centered on the anion vacancy start to extend over the region of the nearest *cations* where $V(r)$ changes its sign.

Along with F^+ and F centers which are well studied experimentally, we have simulated in our previous paper[14] the hypothetical F^- center[25] (an oxygen vacancy with *three* trapped electrons) and concluded that it really could exist; the third electron occupies a local state roughly 1 eV below the conduction band. In this paper we optimized its ground-state geometry and found that the two ions O_1 and O_2 of the same basic O triangle shifted slightly towards the vacancy by $\geq 2\%$ of the O-O distance in a perfect crystal (2.49 Å) and at an angle of 30° with respect to the O-O line (Fig. 1). The nearest cations Al_1 and Al_2 are displaced outwards from the triangle plane by 4% and Al_7 and Al_8 by 2% of the initial Al-O distances in these long and short pairs.

The analysis of the electron density distribution shows that two electrons are well localized inside the O vacancy and occupy a deep local level whereas the third one is delocalized mainly over the nearest Al_7 and Al_8 ions and occupies the above-mentioned level close to the conduction band. This level is split off from the band states since the effective charges (and energy states) of Al_7 and Al_8 cations are considerably altered by a third F^- electron. Qualitatively similar F^- centers (which are negatively charged with respect to the perfect lattice) are known also in alkali halides.[8,26,27]

Using a simple relation between the energies of optical, E_0, and thermal, E_T, ionizations, $E_0 = \epsilon_0 / \epsilon_\infty E_T$,[28] where ϵ_0 and ϵ_∞ are static and high-frequency dielectric constants, we arrive at $E_T = 3.1/9.3 \times 1$ eV ≈ 0.33 eV. In order to estimate roughly the delocalization temperature T_d, one could use the following simple relation: $\tau^{-1} = \nu_0 \exp(E_T/kT_d)$, where ν_0 is the F^- frequency factor and τ is the lifetime of this electron center under efficient destruction. For $E_T = 0.33$ eV, $\nu_0 = 10^{13}$ s^{-1}, and $\tau = 10$ s we estimate the value of $T_d \simeq 125$ K (unlike the 260 K suggested in Ref. 25). For comparison, in alkali halides F^- centers are stable up to the temperatures of 140 K in KBr and 200 K in KCl.[26,27]

We have tried to detect F^- centers experimentally using the stimulation spectra of recombination luminescence. The two main candidates are low-temperature

peaks at 60 and around 100 K. Samples were excited by 6 eV photons from a 250 W deuterium recharge lamp at 80 K during 1 h. However, no photostimulation was observed at 80 K using ir stimulating light with $\lambda > 0.9$ μm. At the same time, such photostimulation has indeed been observed in the interval 3–5 eV, which corresponds to electron release after F-center excitation from the centers responsible for the 260 and 430 K peaks. More detailed studies are planned now, including investigation of defects destroyed at 60 K. (There are no electron and hole centers between 100 and 200 K.)

Calculations of Mg-related F centers support the model of a neutral $F_{Mg} = F^+(Mg^{2+})$ defect rather than a negatively charged $F(Mg^{2+})$ defect. The effect of a Mg atom substituting for an Al nearest to the F^+ center is to lower the absorption and luminescence energies by ~ 0.2 eV; a third absorption band is expected to be around 6 eV.

Up to now only one type of dimer center has been studied, having the two next-nearest-neighbor oxygen vacancies on adjacent basal oxygen planes and thus revealing a high optical anisotropy ($A = a_\parallel / a_\perp \approx 3$).[9] Another kind of dimer center, with the two oxygen vacancies belonging to the same oxygen triangle (i.e., nearest-neighbor vacancies) has not been studied experimentally yet to our knowledge. For both kinds of dimers we found the absorption and luminescence energies to decrease considerably in the series $F_2 \rightarrow F_2^+ \rightarrow F_2^{2+}$ (four, three, and two electrons in the two vacancies, respectively). We expect F_2 centers to have more than the one absorption band observed so far. The agreement of our calculations for the NNN dimer centers with the relevant experimental data,[9] especially for absorption energies, is only qualitative, very likely due to the use of a cluster not big enough for these simulations; even our relatively large 65-atom cluster has three basal planes and thus one of two vacancies lies already at the cluster boundary. Moreover, the effects of electronic polarization are known to be underestimated in the INDO approximation used. Nevertheless, our calculations suggest several important qualitative conclusions on dimer centers. (i) In the series $F_2^{2+} \rightarrow F_2^+ \rightarrow F_2$ the ground-state levels move monotonically up and their excited states are closer and closer to the conduction band. However, for the F_2^{2+} and F_2^+ dimers the excited states are still well localized, whereas the F_2 excited state moves quite close to the conduction band. (ii) Charge distribution analysis for the ground state of NN dimer centers shows that only $0.5e$ of four electrons is delocalized over atoms nearest to the F_2 center, $0.3e$ for the F_2^+ center, and $\sim 0.1e$ for the F_2^{2+} center. That is, the ground-state wave functions of all three centers are well localized. For NNN dimers we have larger values of delocalized electron density—$0.5e$, $0.75e$, and $0.5e$, respectively. The corresponding values for the excited states are $0.9e$, $0.8e$, and $0.3e$ for F_2, F_2^+, and F_2^{2+} NN dimer centers and $1.1e$, $0.8e$, and $0.6e$ for F_2, F_2^+, and F_2^{2+} NNN dimer centers, respectively. The charge distribution analysis shows the increase of electron density delocalization for excited states in comparison to the ground states. (iii) Along with optical transitions in dimer centers whose energies are close to those of

single-vacancy defects (ca. 5.6 eV for F^+, F, and F_2 centers), we expect also for F_2^+ the so-called "M-type" transitions observed earlier in alkali halides and MgO,[8,29−31] and corresponding to the transition between the two molecular orbitals $s(1) \pm s(2)$ which are even and odd with respect to coordinate inversion at the midpoint between vacancies. These energies fall into the ir energy interval (≥ 1 eV) and correspond to the transition shown for F_2^+ centers in Fig. 3 by a bold arrow. In KCl, for example, the absorption energy of the $A_{1g} \rightarrow A_{2u}$ transition is 1.5 eV, to be compared to the F-center absorption observed at 2.35 eV.

ACKNOWLEDGMENTS

*Present address: Institute of Physics, Aarhus University, Denmark.

†Present address: Department of Quantum Chemistry, Uppsala University, Box 518, S-751 20 Uppsala, Sweden.

[1] E. F. Martynovich, V. I. Baryshnikov, and V. A. Grigorov, Opt. Commun. **53**, 257 (1985); Sov. Tech. Phys. Lett. **11**, 81 (1985).

[2] E. R. Hodgson, in *Defects in Insulating Materials,* edited by O. Kanert and J.-M. Spaeth (World Scientific, Singapore, 1993), p. 332.

[3] M. S. Akselrod, V. S. Kortov, D. Ya. Kravetskii, and V. I. Gotlib, Radiat. Protection Dosimetry **32**, 15 (1990).

[4] *Structure and Properties of MgO and Al_2O_3 Ceramics,* edited by W. D. Kingery, Advances in Ceramics Vol. 10 (American Ceramic Society, Columbus, OH, 1983).

[5] J. H. Crawford, Jr., Semicond. Insul. **5**, 599 (1983); Nucl. Instrum. Methods Phys. Res. Sect. B **1**, 159 (1984).

[6] J. Valbis and N. Itoh, Radiat. Eff. Defects Solids **116**, 171 (1991).

[7] L. S. Welch, A. E. Hughes, and G. P. Pells, J. Phys. C **13**, 1805 (1980).

[8] E. Sonder and W. A. Sibley, in *Point Defects in Solids,* edited by J. H. Crawford and L. M. Slifkin (Plenum, New York, 1972), Vol. 1, p. 208.

[9] G. J. Pogatshnik, Y. Chen, and B. D. Evans, IEEE Trans. Nucl. Sci. **NS-34**, 1709 (1987).

[10] K. H. Lee and J. H. Crawford, Jr., Phys. Rev. B **15**, 4065 (1977).

[11] S. Y. La, R. H. Bartram, and R. T. Cox, J. Phys. Chem. Solids **34**, 1079 (1973).

[12] R. C. DuVarney, A. K. Garrison, J. R. Niklas, and J.-M. Spaeth, Phys. Rev. B **24**, 3693 (1981).

[13] S. I. Choi and T. Takeuchi, Phys. Rev. Lett. **50**, 1474 (1983).

[14] A. Stashans, E. Kotomin, and J.-L. Calais, Phys. Rev. B **49**, 14 854 (1994).

[15] P. Deak, J. Giber, and H. Oechsner, Surf. Sci. **250**, 287 (1991); P. Deak, C. R. Ortiz, L. C. Snyder, and J. W. Corbett, Physica B **170**, 223 (1991); P. Deak, L. C. Snyder, and J. W. Corbett, Phys. Rev. B **45**, 11 612 (1992); P. Deak, B. Schröder, A. Annen, and A. Scholz, *ibid.* **48**, 1924 (1993).

[16] E. Stefanovich, E. Shidlovskaya, A. Shluger, and M. Zakharov, Phys. Status Solidi B **160**, 529 (1990); A. L. Shluger, R. W. Grimes, C. R. A. Catlow, and N. Itoh, J. Phys. Condens. Matter **3**, 8027 (1991); A. L. Shluger, E. A. Kotomin, and L. N. Kantorovich, J. Phys. C **19**, 4183 (1986); A. L. Shluger and E. A. Stefanovich, Phys. Rev. B **42**, 9646 (1990); A. L. Shluger, N. Itoh, and K. Noda, J. Phys. Condens. Matter **3**, 9895 (1991).

[17] J. A. Pople and D. L. Beveridge, *Approximate Molecular Orbital Theory* (McGraw-Hill, New York, 1970).

[18] P. W. M. Jacobs, E. A. Kotomin, A. Stashans, E. Stefanovich, and I. Tale, J. Phys. Condens. Matter **4**, 7531 (1992); P. W. M. Jacobs and E. A. Kotomin, Phys. Rev. Lett. **69**, 1411 (1992); P. W. M. Jacobs, E. A. Kotomin, A. Stashans, and I. Tale, Philos. Mag. B **67**, 557 (1993); L. N. Kantorovich, A. Stashans, E. A. Kotomin, and P. W. M. Jacobs, Int. J. Quantum Chem. **52**, 1177 (1994).

[19] J. Lewis, D. Schwarzenbach, and H. D. Flack, Acta Crystallogr. Sect. A **38**, 733 (1982).

[20] M. Causà, R. Dovesi, C. Roetti, E. Kotomin, and V. Saunders, Chem. Phys. Lett. **140**, 120 (1987).

[21] L. Kantorovich and A. Livshicz, Phys. Status Solidi B **174**, 79 (1992).

[22] L. Kantorovich, E. Heifets, A. Livshicz, M. Kuklja, and P. Zapol, Phys. Rev. B **47**, 14 875 (1993).

[23] M. Born and K. Huang, *Dynamic Theory of Crystalline Lattices* (Oxford University Press, London, 1954).

[24] P. A. Kulis, M. J. Springis, I. A. Tale, V. S. Vainer, and J. A. Valbis, Phys. Status Solidi B **104**, 719 (1981); P. A. Kulis, M. J. Springis, I. A. Tale, and J. A. Valbis, Phys. Status Solidi A **53**, 113 (1979); M. J. Springis and J. A. Valbis, Phys. Status Solidi B **123**, 335 (1984).

[25] V. S. Kortov, T. S. Bessonova, M. S. Akselrod, and I. I. Milman, Phys. Status Solidi A **87**, 629 (1985).

[26] M. Hirai, M. Ikezawa, and M. Ueta, J. Phys. Soc. Jpn. **17**, 724 (1962); **17**, 1483 (1962).

[27] M. Hirai and A. B. Scott, J. Chem. Phys. **44**, 1753 (1966).

[28] N. F. Mott and R. W. Gurney, *Electronic Processes in Ionic Crystals* (Oxford University Press, Oxford, 1940).

[29] R. A. Evarestov, Opt. Spectrosc. **16**, 198 (1964); Phys. Status Solidi B **31**, 401 (1969); A. D. Kashkai, A. A. Berezin, A. N. Arsenjeva-Geil, and M. S. Matveev, *ibid.* **54**, 113 (1972).

[30] J. H. Crawford, Jr., and L. M. Slifkin, in *Point Defects in Solids* (Ref. 8), p. 381.

[31] B. Henderson, Crit. Rev. Solid State Mater. Sci. **9**, 1 (1980).

FIG. 1. Top view of the stoichiometric quantum cluster used in the calculations. It contains 13 structural elements (SE's); each SE includes a five-ion oxygen triangle and two Al atoms situated symmetrically above and below the triangle, on the z axis perpendicular to the triangle plane. The cluster consists of three basal planes shown in white, dots (2.17 Å below the xy plane), and gray (2.17 Å above the xy plane), respectively. In F-type defect calculations the ion O_3 was replaced by a vacancy. Dimer centers contain two NN and NNN vacancies on adjacent planes (see Figs. 2 and 3 below for more details).